

**Jul.2012 / Vol.138**

MITSUBISHI ELECTRIC

# ADVANCE

High-Frequency and Optical Devices

• **Editorial-Chief**

*Shoichiro Hara*

• **Editorial Advisors**

*Toshio Masujima  
Maki Ikegami  
Kazuhiro Oka  
Tetsuji Sorita  
Chikao Nishida  
Hideaki Okada  
Takahiro Nishikawa  
Tetsuyuki Yanase  
Ichiro Fujii  
Taizo Kittaka  
Masato Nagasawa  
Daisuke Kawai  
Keiichiro Tsuchiya  
Toshitaka Aoyagi*

• **Vol. 138 Feature Articles Editor**

*Hiroyuki Joba*

• **Editorial Inquiries**

*Kazuhiro Oka  
Corporate Total Productivity Management  
& Environmental Programs  
Fax +81-3-3218-2465*

• **Product Inquiries**

**NORTH AMERICA**

Mitsubishi Electric & Electronics USA, Inc.  
Semiconductor Division  
5201 Great America Parkway, Suite 332  
Santa Clara, CA 95054, USA  
*Julie Callaghan*  
FAX +1-408-727-2689

**GERMANY**

Mitsubishi Electric Europe B.V. German  
Branch Semiconductor European  
Business Group  
Gothaer Str. 8 40880 Ratingen, Germany  
*Judith Seifert*  
Fax +49-(0)2102-486 4140

**CHINA**

Mitsubishi Electric & Electronics (Shanghai)  
Co.,Ltd  
29 Floor, Shanghai MAXDO Center No.8,  
Xing Yi Road, Hong Qiao, Shanghai  
200336, China  
*Qian Yu Feng*  
FAX +86-21-5208-1502

**Mitsubishi Electric Advance** is published on  
line quarterly by Mitsubishi Electric  
Corporation.  
Copyright © 2012 by Mitsubishi Electric  
Corporation; all rights reserved.  
Printed in Japan.

The company names and product names described herein are the  
trademarks or registered trademarks of the respective companies.

**CONTENTS**

**Technical Reports**

Overview .....1  
by *Masaki Sakuyama*

Three-mode Stage-bypass High-efficiency Power Amplifiers for  
Wideband Code Division Multiple Access (W-CDMA) Applications  
.....2  
by *Kenichi Horiguchi, Kazuya Yamamoto and Masatoshi Nakayama*

GaN HEMT Amplifier for C-band Space Applications .....5  
by *Takashi Yamasaki, Hiroaki Minamide and Atsushi Hasuike*

Development of High-power MOSFET Device for Professional  
Radio Applications .....9  
by *Kazuhito Mori, Yoji Maruyama and Koichi Fujita*

Optical Module for 10 Gigabit Ethernet Passive Optical Network  
(10 G-EPON OLT) .....12  
by *Satoshi Shirai, Nobuo Ohata and Masaki Noda*

High-power 638 nm Semiconductor Laser Diode for Small Color  
Projectors .....16  
by *Takehiro Nishida, Harumi Nishiguchi and Naoyuki Shimada*

# Overview



Author: *Masaki Sakuyama\**

## High-Frequency and Optical Devices as Key Devices for Information and Communication Technology (ICT)

In recent years, the amount of communication traffic has been growing due to significant progress in broadband communications. In the fields of both wireless communications such as mobile phones and optical communications such as fiber optical transmission, continuous research and development are under way to raise the transmission rate, including: faster data transmission through the mobile telephone network, applications of GaN devices to the communications infrastructure, transition from 1 Gbps to 10 Gbps optical communication system for FTTH, and speeding up of long-distance communications from 40 Gbps to 100 Gbps. As key devices for information and communication technology (ICT), high-frequency and optical devices will play an even more important role.

This issue presents the results of product development by Mitsubishi Electric in these fields.

# Three-mode Stage-bypass High-efficiency Power Amplifiers for Wideband Code Division Multiple Access (W-CDMA) Applications

Authors: Kenichi Horiguchi\*, Kazuya Yamamoto\*\* and Masatoshi Nakayama\*

We have developed a 3.4-V, 1.95-GHz band stage-bypass power amplifier capable of operating in three power modes. This amplifier switches the signal path to use different transistors and circuit configurations for high, medium and low power modes. The new amplifier satisfies the distortion specifications of the wideband code division multiple access (W-CDMA), while achieving superior performance of power added efficiency (PAE) of 40%, 23% and 12% at high, medium and low power mode, respectively.

## 1. Introduction

In the W-CDMA mobile phone system, each terminal emits radio waves at a different strength depending on the distance from the base station and/or transmission condition. Therefore, the power amplifier is required to achieve good efficiency in each power mode corresponding to a different transmission power, i.e., high, medium or low power mode. For these reasons, various techniques have been used in recent mobile phones such as using a DC/DC converter with a variable output voltage<sup>(1)</sup>, and switching multiple power amplifiers or paths having different output levels<sup>(2)</sup>. Meanwhile, in a terminal, a transmission wave that is emitted from the power amplifier to the receiving unit may cause coupling loop interference for the received signal. Therefore, the high-power amplifier is required to reduce the output power level in the receiving frequency band. This paper presents the results of developing the stage-bypass power amplifier, which achieves high power efficiency for each of the three power modes by changing the signal path and switching the transistors and circuit configurations.

## 2. Circuit Configuration

Figure 1 shows the circuit configurations of conventional and newly developed three-mode stage-bypass power amplifiers. The developed amplifier consists of high-frequency power transistors (Tr1, Tr2 and Tr3) which are switched by the switches (SWs) corresponding to the high, medium or low power mode.

Tr1, Tr2 and Tr3 are bipolar field effect transistors (BiFETs), and SWs perform on/off control to change the signal path for each of the three power modes, and thus the transistors and matching circuits corresponding to each power mode are selected. Each of the output matching circuits is tuned to provide fundamental and second harmonic load impedances optimized for both output power and efficiency. This amplifier has a built-in transistor bias circuit and a control circuit for determining the on/off state of each switch. In the conventional configuration, the total loss of the output circuit is determined by the sum of the loss of switch SW6 and that of the matching circuit disposed after the final-stage power transistor Tr3. The loss of switch SW6 can be reduced by increasing the switch size, but this increases the semiconductor chip size. In the newly developed configuration, there is no switch after transistor Tr3, and thus the loss of the output circuit can be reduced. In addition, the output switch itself has been eliminated. The size of the new amplifier is  $3.0 \times 3.0 \text{ mm}^2$ .

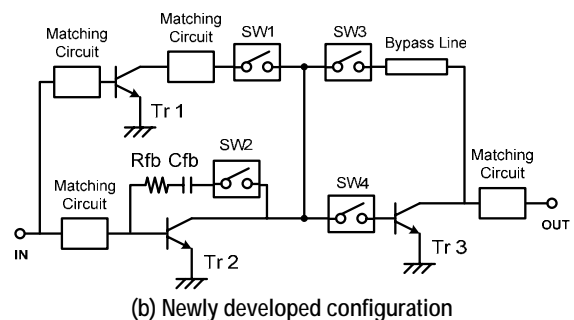
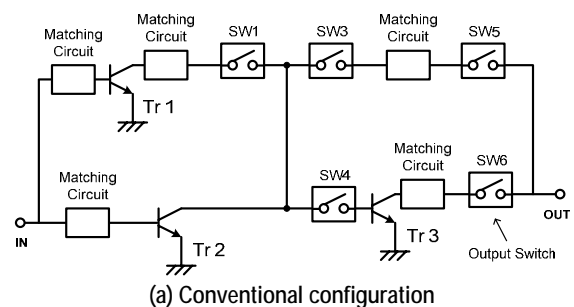


Fig. 1 Schematic diagrams of three-mode stage-bypass power amplifiers

Figure 2 shows the amplifying paths of high-frequency signals for the three power modes. In the high power mode (Fig. 2 (a)), transistor Tr1 and switches SW1 and SW3 are off, and the high-frequency input signal is amplified through the path from Tr2 to Tr3. In this mode, SW2 is on, and thus Tr2 operates as a feedback amplifier. In the medium power mode (Fig. 2 (b)), transistors Tr1 and Tr3 and switches SW1, SW2 and SW4 are off, and the input signal is amplified in the path from Tr2 through the bypass line. In this mode, SW2 is off and thus the feedback circuit of Tr2 is disabled. In the low power mode (Fig. 2 (c)), transistors Tr2 and Tr3 and switches SW2 and SW4 are off, and thus the input signal is amplified in the path from Tr1 through the bypass line.

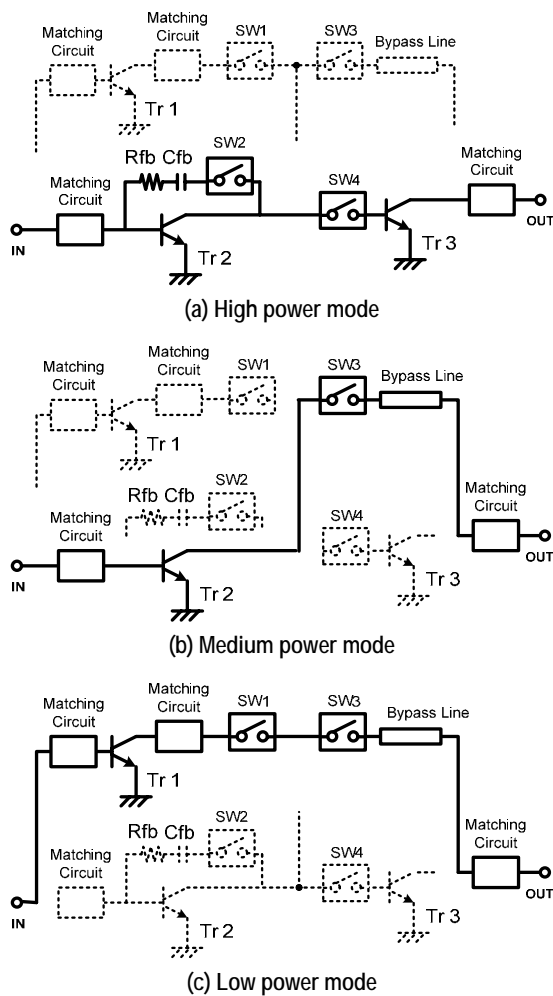


Fig. 2 Signal path of each power mode

Figure 3 shows the relationship between the feedback resistance ( $R_{fb}$ ) and the receiver band noise, that is, a power leakage from the transmitter into the receiver band (2,110 – 2,170 MHz). The power leakage level was calculated by simulating the amplification of a 1.95 GHz signal in the high power mode. In contrast to the receiver band noise level of  $-136.4$  dBm/Hz without a feedback circuit, if the feedback circuit is connected

and the feedback resistance is set to  $1,000 \Omega$  or lower, the receiver band noise can be reduced to  $-137$  dBm/Hz or lower. If the feedback circuit is activated, however, the amplifier gain is also reduced. Therefore, in the newly developed amplifier, SW2 is controlled to activate the feedback circuit only in the high power mode to suppress the receiver band leakage power in this operation mode.

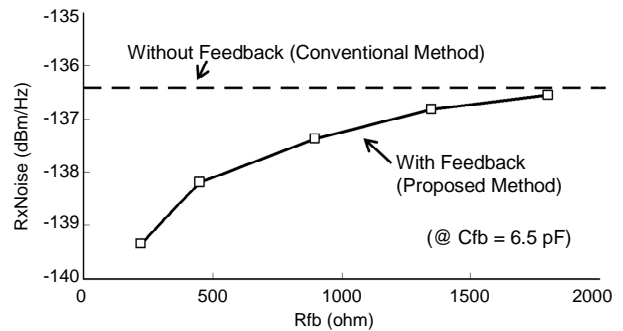
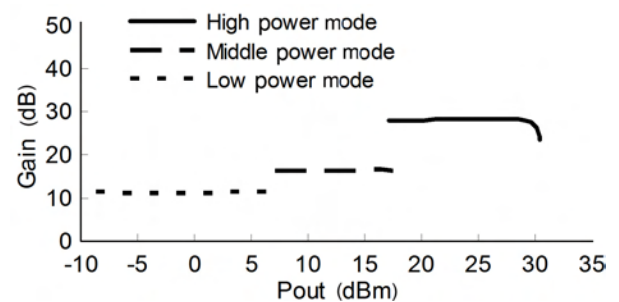
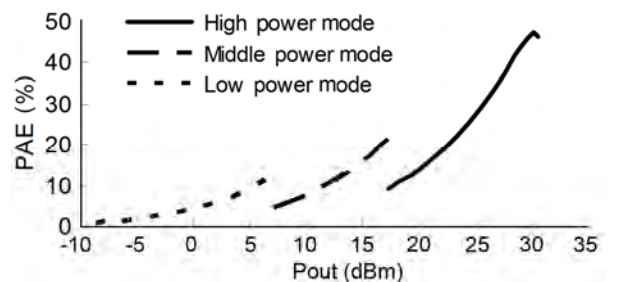


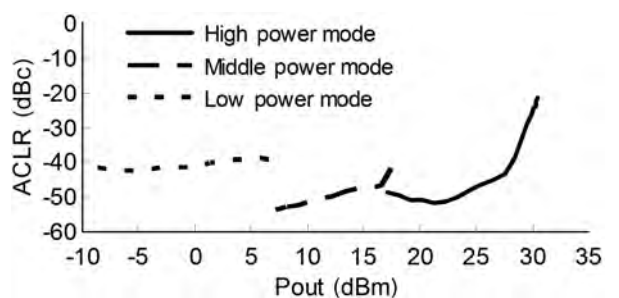
Fig. 3 Relationship between feedback resistance and receiver band noise



(a) Gain characteristics



(b) Power added efficiency characteristics



(c) ACLR characteristics

Fig. 4 Measured gain, PAE and ACLR characteristics of developed amplifier by inputting W-CDMA signals

### 3. Evaluation Result

Figure 4 shows the new amplifier's characteristics of the gain, PAE and adjacent channel leakage power ratio (ACLR). The measurements were made at an operating voltage of 3.4 V, with an input of a 1.95 GHz W-CDMA signal. The achieved performances are: gain of 28.3 dB, PAE of 42% and ACLR of -39 dBc in the high power mode with an output of 28.4 dBm; gain of 16.4 dB, PAE of 22% and ACLR of -42 dBc in the medium power mode with an output of 17.5 dBm; and gain of 11.3 dB, PAE of 13% and ACLR of -40 dBc in the low power mode with an output of 7.4 dBm. The measurement result of the receiver band noise level is -136 dB/Hz.

### 4. Conclusion

A 1.95 GHz band stage-bypass power amplifier for W-CDMA applications has been developed, and good efficiency has been confirmed in each of the three output power modes of high, medium and low.

We plan to further improve the efficiency and reduce the cost of the amplifier. In addition to the single-band product, we also plan to develop a product for multi-band operation.

### References

- (1) Teeter, D. A., et al.: Average Current Reduction in (W)CDMA Power Amplifiers, IEEE Radio Frequency Integrated Circuits Symposium Digest, 429-432 (2006)
- (2) Hau, G., et al.: Multi-Mode W-CDMA Power Amplifier Module with Improved Low-Power Efficiency using Stage-Bypass, IEEE Radio Frequency Integrated Circuits Symposium Digest, 163-166 (2010)

# GaN HEMT Amplifier for C-band Space Applications

Authors: Takashi Yamasaki\*, Hiroaki Minamide\* and Atsushi Hasuike\*

## 1. Introduction

With the diversifying functions and increasing traffic of recent satellite communications, the amplifiers installed in satellites must provide higher power and improved efficiency. Commonly-used satellite-mounted amplifiers are, in general, either traveling wave tube amplifiers (TWTAs) or solid state power amplifiers (SSPAs) using gallium arsenide field-effect transistors (GaAs FETs). However, because of this high output power and high efficiency, TWTAs are used more often than SSPAs. Meanwhile, the gallium nitride high electron mobility transistor (GaN HEMT) is expected to improve the output power and efficiency of SSPAs. Owing to its material properties, the GaN HEMT is capable of high voltage operation and produces a high power density, and thus is expected to be a high-frequency device that realizes a high-power and high-efficiency SSPA, and in recent years, high-power GaN HEMT amplifiers are being developed at many research institutions<sup>(1)(2)(3)(4)</sup>.

This time, based on Mitsubishi Electric's GaN HEMT device, we have developed a high-power and high-efficiency amplifier transistor, and verified that it provides sufficient reliability for satellite applications.

## 2. GaN HEMT High-Power Amplifier

### 2.1 Transistor characteristics

Mitsubishi Electric's GaN HEMT, which is used for the newly developed high-power amplifier, has the following structure-related advantages: (i) current collapse suppression and good pulse I-V characteristics by forming a passivation film using a catalytic chemical vapor deposition (Cat-CVD) process<sup>(5)</sup>, and (ii) low on-resistance by reducing the resistance of ohmic contact using a silicon (Si) ion implantation process.

Figure 1 shows the output characteristics of the unit cell transistor. The evaluated element has gate dimensions of 0.6  $\mu\text{m}$  in length and 1.2 mm in width, and the measurements were performed under the continuous wave (CW) condition at a C-band frequency (4 GHz) with a drain voltage  $V_d = 40$  V, and a drain current  $I_d$  (RFOff) = 50 mA/mm. The load and source impedances were determined so as to maximize the power added efficiency (PAE) at the fundamental and second harmonic frequencies. Under these conditions, the measurements of the unit cell element confirmed

the superior performance of Mitsubishi Electric's GaN HEMT, that is, a PAE of 80% and output power density of 3.3 W/mm.

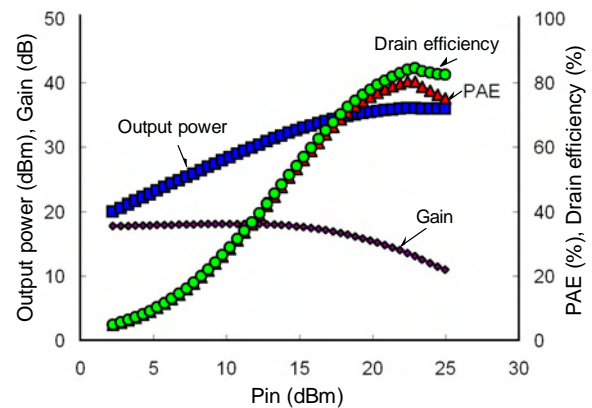


Fig. 1 Output characteristics of unit cell transistor

### 2.2 Design of internal matching circuit

To develop a high-power and high-efficiency amplifier using a high-performance transistor, it is important to optimize the matching circuit. The amplifier circuit was designed to minimize the matching circuit loss and optimally deal with the fundamental and harmonic (especially second harmonic) frequencies. Figure 2 shows the circuit configuration of the C-band 100-W output internally matched FET amplifier. Four GaN HEMT chips with a narrow gate width are combined in parallel to achieve a high output gain, and both the input and output matching circuits are configured with two-stage quarter-wave transmission line transformers

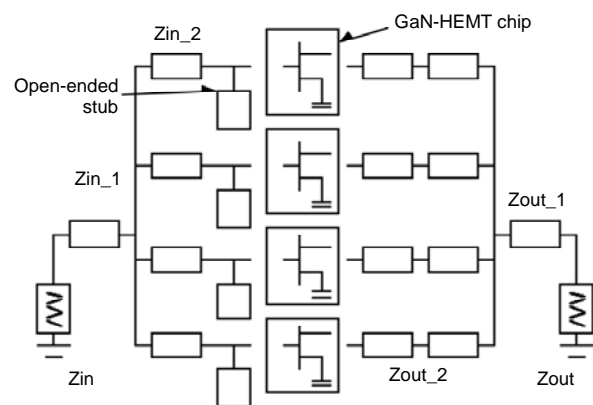


Fig. 2 Circuit configuration of C-band 100-W output internally matched FET amplifier

to enhance the bandwidth. The source load at the second harmonic frequency significantly influences the efficiency, and thus it is optimized by using open-ended stubs located nearby the chip. The pattern layout of the output matching circuit is optimized so as to reduce the circuit loss.

Using the same technique, additional internal matching circuits were designed for the 20 W and 40 W output single-chip amplifiers.

### 2.3 Evaluation results of electrical characteristics

Figure 3 shows a photograph of the inside of the “MGFC50G3742S,” the 100-W output internally matched FET amplifier.

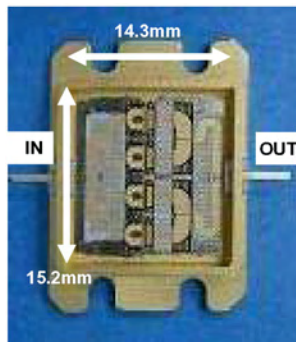


Fig. 3 Internal view of MGFC50G3742S (100 W model)

The cavity size of the package is 14.3 × 15.2 (mm), which are the same dimensions as Mitsubishi Electric’s GaAs 25-W amplifier. Four GaN HEMT chips and matching circuit boards are implemented inside the hermetically sealed package. The GaN HEMT chips are configured in parallel with a total gate width of 9.6 mm; and the input matching circuit board is configured in two stages on the aluminum and high permittivity substrates, while the output matching circuit board is in three stages on the aluminum and high permittivity substrates.

Figure 4 shows the output characteristics measured under the CW condition at a frequency of 4 GHz,

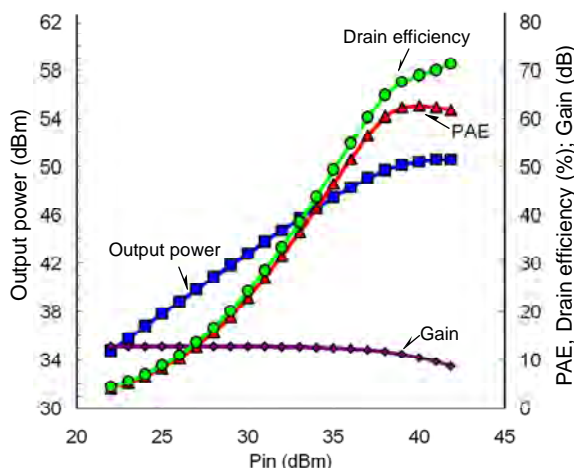


Fig. 4 Output characteristics of MGFC50G3742S (100 W model)

$V_d = 40$  V, and  $I_d$  (RFOff) = 2 A. This device has achieved industry-leading performance, namely, an output power at 2 dB gain compression point, P2dB, of 50 dBm, actual gain, Gp, of 11.4 dB, and power added efficiency, PAE, of 62%. Table 1 summarizes the product specifications of the commercialized C-band GaN internally matched FET amplifiers.

Table 1 Product lineup of C-band GaN internally matched FET amplifiers

Model name: MGFC-		50G3742S	46G3742S	43G3742S
Recommended conditions	Vds	40V	40V	40V
	Ids (RFOff)	2.0A	1.0A	0.5A
	Rg	10Ω	25Ω	50Ω
Frequency	Freq.	3.7-4.2 GHz*	3.7-4.2 GHz*	3.7-4.2 GHz
Power at 2 dB gain compression point	P2dB (typ.)	100W	40W	20W
Linear power gain	Glp (typ.)	13dB	14dB	14dB
Power added efficiency	PAE (typ.)	60%	60%	60%
External dimensions (mm)		17.4 × 24.0 × 4.3		

\*Frequency band is divided into two bands.

### 3. Reliability Tests for Space Applications

For space applications, it is vital to verify the reliability when the device is used in outer space. In general, reliability tests are performed on the long-term life, mechanical properties, etc. Mitsubishi Electric has conducted reliability tests under the conditions listed in Table 2.

Table 2 Reliability test items

Category	Item	Test conditions	Result
Mechanical test	Mechanical	Temperature cycling Vibration/ Shock Constant acceleration, etc.	No failure
Life test	MTTF (C.L.90%)	Tch = 250°C Vds = 47V	2,000 hrs
		Tch = 260°C Vds = 47V	1,000 hrs
		Tch = 270°C Vds=45V	832 hrs
	RF Life	Tch = 230°C Vds = 45V @P2dB 1,000 hrs	No failure
DC Life	Tch = 230°C Vds = 45V 5,000 hrs	No failure	
	Radiation test	Single event burnout (RF) Vds = 45V Pout = P2dB→P13dB (DC) Vds = 175V, Vgs = -5V Br ion for each test LET: 31.2 MeV/(mg/cm <sup>2</sup> ) Fluence: 1×10 <sup>6</sup> ions/cm <sup>2</sup>	No failure
	Total dose effect	12 Mrad of Co 60 γ-rays during DC operation with Vds = 45V	No failure

LET: Linear Energy Transfer

The -65°C/ 175°C temperature cycling test, 1,500 G vibration test, and other mechanical tests assuming

the physical stresses in outer space were performed, and no failures were observed.

To determine the mean time to failure (MTTF: mean time to a component failure without maintenance), which numerically represents the product's life time, a temperature accelerated test was performed on the 20-W output amplifiers operated at  $V_{ds} = 47$  V, and channel temperature ( $T_{ch}$ ) = 250/ 260°C. The calculation result indicates that the activation energy ( $E_a$ ) is 1.62 eV, which ensures a high reliability with a life time of one million hours under the operating conditions of  $T_{ch} = 175^\circ\text{C}$  and  $V_{ds} = 45$  V. Figure 5 depicts the calculation result of MTTF.

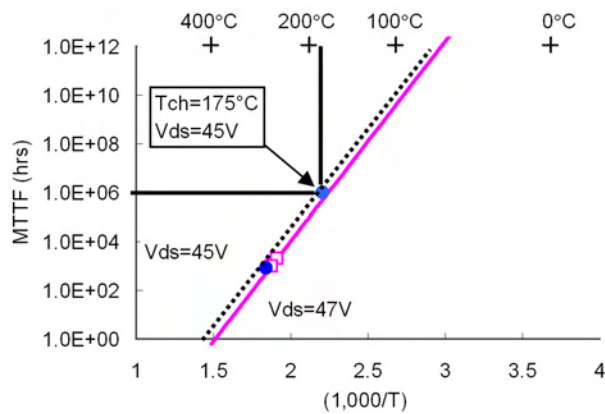


Fig. 5 Calculation result of MTTF

We have also conducted direct current (DC) and radio frequency (RF) life tests as a part of the long-term life tests. The results of these life tests are shown in Figs. 6 and 7 (only P2dB data are shown). In these charts, the horizontal axis indicates the time, and the vertical axis indicates the variation in the device property. In these tests, the deterioration in P2dB is judged based on the criterion of  $\pm 1$  dB. The DC life test was carried out under the conditions of  $T_{ch} = 230^\circ\text{C}$  and  $V_{ds} = 45$  V, and the variation in P2dB after 5,000 hours indicated a satisfactory level of equal to or less than 0.5 dB. The RF life test was carried out under the conditions of  $T_{ch} = 230^\circ\text{C}$ ,  $V_{ds} = 45$  V, and an input power giving P2dB, and the variation in P2dB after 1,000 hours was sufficiently low at 0.2 dB or less.

The radiation tests were performed on the single event burnout and total dose effect, where high-energy heavy ions impinge on the semiconductor element, causing an instantaneous change in the electrode potential, resulting in an overvoltage or overcurrent flowing in the FET and the element may burn out (single event burnout), or accumulated radiation dose may cause deterioration of the semiconductor element (total dose effect). In the former test, Br ions were irradiated during the DC (pinch off) operation as well as during the RF operation where the output power was varied from the 2 dB gain compression point to the 13 dB gain

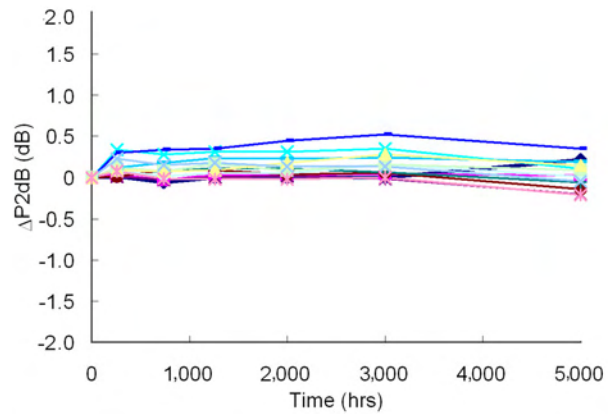


Fig. 6 DC life test result (variation of P2dB)

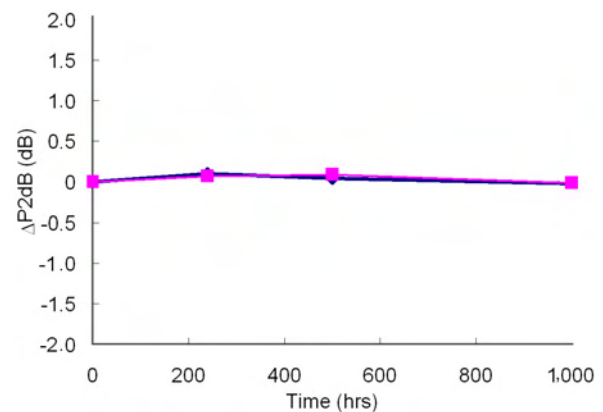


Fig. 7 RF life test result (variation of P2dB)

compression point, and no element failures were observed in either case. In the latter test, cobalt 60  $\gamma$ -rays were irradiated during the DC operation, causing no element failures.

The results of all the reliability tests are satisfactory, indicating sufficient reliability for the device to be used in outer space.

#### 4. Conclusion

Using Mitsubishi Electric's GaN HEMT, C-band high-power amplifiers for space applications have been developed. By minimizing the loss of the matching circuit itself and optimally treating the fundamental and harmonic (especially second harmonic) frequencies, industry-leading performance of 100 W power output and PAE of 62% under the CW condition has been achieved. In addition, various reliability tests were conducted assuming the conditions for satellite applications, and satisfactory results were obtained.

This time, we have commercialized a range of GaN HEMT C-band amplifiers with 20, 40, or 100-W internally matched FETs and 2-W output discrete FET device. The newly developed products provide high performance rivaling the TWTA, which has advantages of high power output and high efficiency, and will contribute to the development of a compact and lightweight SSPA.

## References

- (1) Iyomasa, K., et al.: GaN HEMT 60 W Output Power Amplifier with Over 50% Efficiency at C-Band 15% Relative Bandwidth Using Combined Short and Open Circuited Stubs, 2007 IEEE MTT-S Int. Microwave Symp. Dig., TH1A-3 (2007)
- (2) Otsuka, H., et al.: Over 57% Efficiency C-band GaN HEMT High Power Amplifier with Internal Harmonic Manipulation Circuits, 2008 IEEE MTT-S Int. Microwave Symp. Dig. WE1E-03 (2008)
- (3) Shigematsu, H., et al.: C-band 340-W and X-band 100-W GaN Power Amplifiers with Over 50% PAE, 2009 IEEE MTT-S Int. Microwave Symp. Dig. 1265–1268 (2009)
- (4) Yamasaki, T., et al.: A 68% Efficiency, C-Band 100 W GaN HEMT Amplifier for Space Applications, 2010 IEEE MTT - S Int. Microwave Symp. Dig. TH3D-1 (2010)
- (5) Yoshitaka Kamo, et al.: A C-band AlGaIn/GaN HEMT with Cat-CVD SiN Passivation Developed for an Over 100W Operation, Mitsubishi Denki Giho, 80, No. 5, 333–336 (2006) (in Japanese)

# Development of High-power MOSFET Device for Professional Radio Applications

Authors: Kazuhito Mori\*, Yoji Maruyama\*\* and Koichi Fujita\*\*\*

With the progress of digitization, miniaturization, lower power consumption and cost reduction, professional radios requires a power amplification device in a surface mount package with a higher performance.

In response to these requirements, a 12.5-V operation high-power MOSFET, the RD70HUF2, has been developed.

The newly developed device has achieved industry-leading high-frequency performance: typical output power of 75 W and drain efficiency of 65% at a frequency of 530 MHz.

## 1. Introduction

Recent professional radio technologies are making significant progress toward a digital transmission system such as terrestrial trunked radio (TETRA) as well as for lower power consumption and smaller radios. Therefore, electric power amplification devices for the transmitting stage are required to further reduce distortion and enhance efficiency.

Meanwhile, the package of electronic components used for professional radios is shifting to the surface mount type to facilitate production automation. The electric power amplification devices for the transmitting stage are also required to shift from manual- to surface-mounting type to permit automation.

To meet these requirements, Mitsubishi Electric has developed the RD70HUF2, a surface mountable, 12.5-V operation high-power discrete MOSFET device for use in professional radios for mobile vehicles, and mass production started this year.

We have developed a device package that enables a high-power device to be surface-mounted on the circuit board to dissipate the generated heat through the heat sink of the radio chassis, and a transistor that can be used in professional digital radios in both the VHF and UHF bands.

## 2. Structure of the Device Package

The device package for conventional high-power MOSFET is formed with a metal flange and ceramic cap, whereas the RD70HUF2 uses a surface mountable plastic molded package to enable automated production of radio sets. Figure 1 is a photograph of the external package and Fig. 2 shows its internal structure.

Even if the device is surface-mounted on the circuit

board, the newly developed package frame can dissipate the heat being generated by the MOSFET chip through the heat sink on the radio chassis.

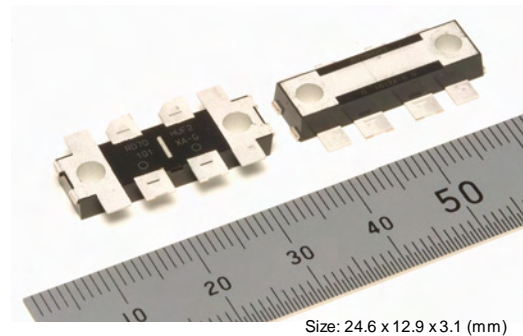


Fig. 1 External view of RD70HUF2

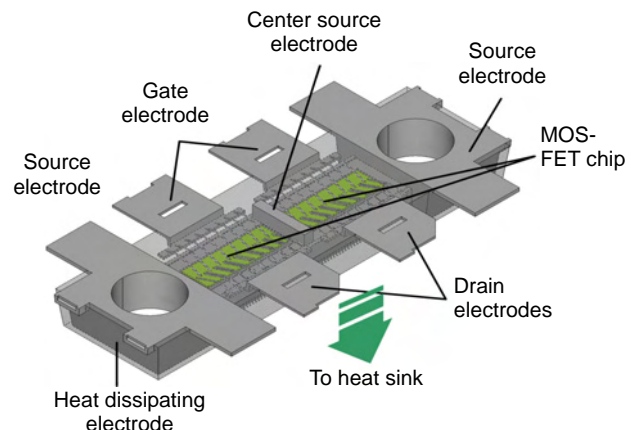


Fig. 2 Structure of package frame

The base frame of this package consists of thin-plate source electrodes and a thick-plate heat dissipating electrode formed into a single piece, and thus the base frame varies in thickness and is difficult to be made by general press forming. This time, we have achieved single-piece forming by using a method of sintering metallic powder.

## 3. Structure of Transistor

Mitsubishi Electric has been working on the development of MOSFET structures using a silicon wafer to achieve high power output, high efficiency, ruggedness to VSWR mismatch, and low distortion<sup>(1)(2)(3)</sup>. By integrating these technologies, we have developed a new MOSFET chip. The cross-sectional structure of the new MOSFET is shown in Fig. 3.

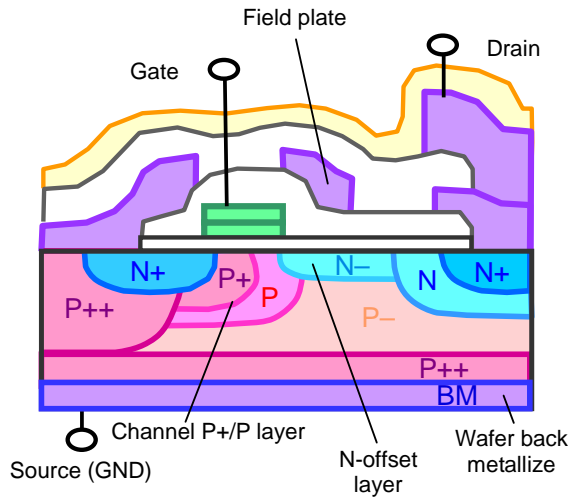


Fig. 3 Cross-sectional structure of MOSFET

For this MOSFET, a thinner wafer and improved wafer back metallization are used to reduce the thermal resistance and ground resistance, and thus higher power output and enhanced efficiency have been achieved. In addition, low distortion has also been achieved by taking advantage of the impurity concentrations in the channel P+/P and N- offset regions and the filed plate, which reduce drain conductance, output capacitance, and feedback capacitance, as these are the causes of degrading distortion.

For the wideband operation, the device must also provide a high gain in the UHF band and high load mismatch tolerance in the VHF band. For this chip, the gain has been improved by reducing the gate length, and the high load mismatch tolerance has also been enhanced by using the drain N region and the P- region of the silicon wafer as a diode to release the reflected power to the back side of the chip.

Figure 4 is an external view of the MOSFET chip. With these improvements in the MOSFET structure, high-frequency characteristics exceeding those of conventional products have been achieved.

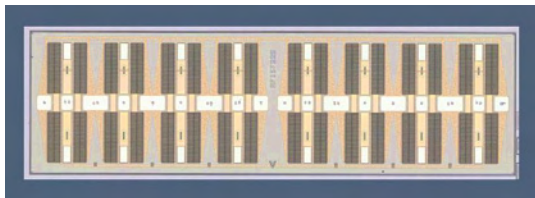


Fig. 4 External view of MOSFET chip

#### 4. Device Evaluation Board

The circuit design and its implementation are essential for fully utilizing the MOSFET performance in the power amplifier for the radio transmitting stage.

To support the design and implementation of the circuit using RD70HUF2, evaluation boards corresponding to various radio applications have been developed. Figure 5 shows one of those device evaluation boards.

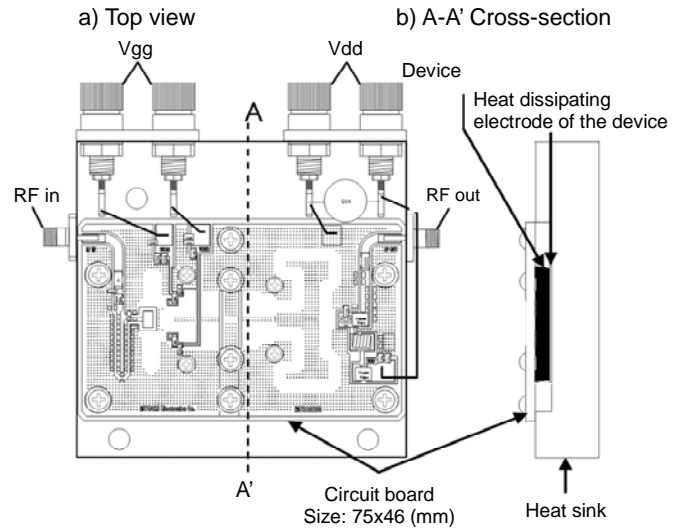


Fig. 5 Evaluation board for sales promotion of the device

This evaluation board is a power amplifier consisting of one unit of the new device and additional components, which are surface-mounted on the printed circuit board (PCB) to configure the amplifier circuit, and then attached to the heat sink.

The PCB size of this evaluation board is reduced by approximately 80% from Mitsubishi Electric's conventional evaluation board. In designing the amplifier circuit of the radio, this board will help the customer shorten the design period.

#### 5. Basic High-Frequency Characteristics

Tables 1 and 2 compare basic high-frequency characteristics between Mitsubishi Electric's conventional and newly developed products. For the new device, the listed high-frequency characteristics are those when it is implemented on the above-described evaluation board. In the VHF band, the saturation power is improved by approximately 10 W from the level of the conventional product, while in the UHF band, the power gain is improved by approximately 4 dB from the conventional product. In addition, the drain efficiency is improved by 5% or more at the same power setting.

Table 1 Comparison in VHF band with conventional Mitsubishi Electric product

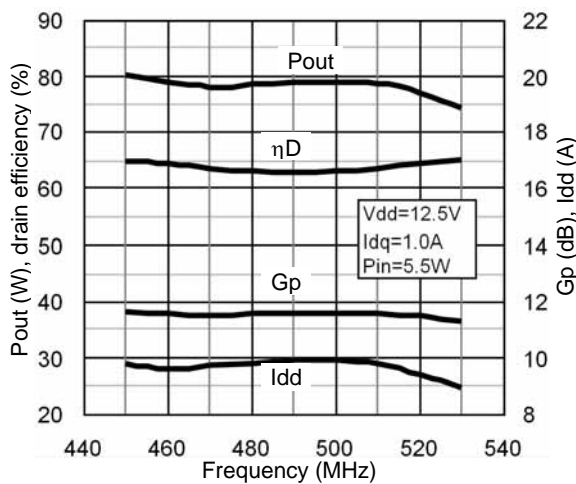
Item	Condition	Conventional	Newly developed
Frequency for VHF evaluation	175 MHz	RD70HVF1	RD70HUF2
Saturation power	at 4 W input	83W	93W
Drain efficiency	at 4 W input	58%	67%

**Table 2 Comparison in UHF band with conventional Mitsubishi Electric product**

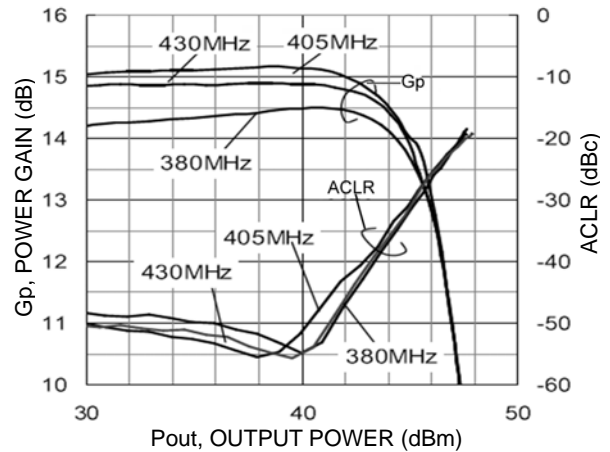
Item	Condition	Conventional	Newly developed
Frequency for UHF evaluation	520 MHz	RD60HUF1	RD70HUF2
Power gain	at 70 W output	8dB	12dB
Drain efficiency	at 70 W output	58%	63%

Figure 6 shows the frequency dependence in the UHF band. In the UHF band, under the band matching condition between 450 and 520 MHz with an input power of 5.5 W, an output power equal to or more than 75 W and a drain efficiency equal to or more than 63% have been achieved. It should be noted, in particular, that the high-frequency characteristics with a power output of 75 W (typ) and a drain efficiency of 65% (typ) at a frequency of 530 MHz is the best performance in the industry.

Figure 7 shows the output power dependence of the power gain and adjacent channel leakage ratio (ACLR) when a digital modulation signal for UHF professional radios is used. In the range from linear opera-



**Fig. 6 High-frequency characteristics matching the UHF professional radio band**



**Fig. 7 Measurement results of power gain and ACLR characteristics**

tion to 3 dB gain compression point with an output power of 40 dBm, a high performance with a power gain of 15 dB and ACLR of -50 dBc has been achieved. These high performances can significantly help to improve the characteristics of professional digital radios.

We will continue to develop high-performance MOSFET devices in response to the evolution of professional radio and other mobile communications, thus improving the performance and reducing the cost of the radio equipment.

**References**

- (1) Shinya Oida, et al.: Simulation of RF MOSFET Devices, Mitsubishi Denki Giho, Vol. 70, No. 2, 141-184 (1996). (in Japanese)
- (2) Koichi Fujita, et al.: Radio-Frequency High-Power RF MOSFET, Mitsubishi Denki Giho, Vol. 74, No. 6, 397-400 (2000). (in Japanese)
- (3) Koichi Fujita, et al.: C-11-9 Improvement of Drain Efficiency in LDMOSFET for Base Station, Proceedings of IEICE General Conference, 2003, Electronics (2), 69, March 3, 2003 (in Japanese)

# Optical Module for 10 Gigabit Ethernet Passive Optical Network (10 G-EPON OLT)

Authors: Satoshi Shirai\*, Nobuo Ohata\* and Masaki Noda\*

## 1. Introduction

In response to growing internet traffic, the GE-PON system is becoming more widely used as an economic and high-speed fiber to the home (FTTH) service. To enable the broadcasting of ultra-high definition television and other services in the future, it is necessary to expand the capacity of the optical access network, in which 10 Gigabit Ethernet passive optical network (10G-EPON), the next-generation optical access system, is expected to play an increasingly important role. With this background, in IEEE 802.3av, the international standard for optical access systems, 10 G-EPON was standardized in September 2009. For smooth transition from GE-PON, coexistence of GE-PON and 10G-EPON on the same existing optical distribution network is required. Therefore, the optical line terminal (OLT) as the central office equipment is required to have all the functions of a 10.3 Gbps transmitter, 1.25 Gbps transmitter, 10.3 Gbps receiver, and 1.25 Gbps receiver. We have developed a triplexer module in which all of these functions are integrated for the 10 G-EPON OLT. This paper describes the design and evaluation results of the triplexer module.

## 2. Configuration and Design of Optical Module for 10 G-EPON OLT

### 2.1 Configuration

Figure 1 shows the configuration of the triplexer module. The 10.3 Gbps transmitter uses an electroabsorption modulator integrated laser diode (EA-LD) with a wavelength of 1.577  $\mu\text{m}$ . The modulator in the EA-LD has an optimized quantum well structure to enhance the output, achieving a high power output, high extinction ratio, and low chirp characteristic. In addition, a new CAN package has been developed and applied to achieve a small module size and low cost<sup>(1)</sup>. The CAN package is equipped with glass feedthroughs that cover the lead pins and are structured to prevent multiple electrical reflections between EA-LDs to convey 10.3 Gbps high-frequency signals into the EA-LD without loss. The characteristics of the EA-LD greatly depend on the temperature, and thus a small thermo electric

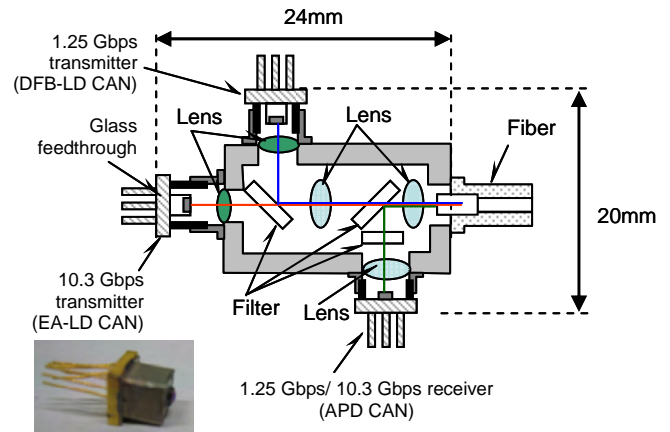


Fig. 1 Configuration of triplexer module

cooler (TEC) is built-in to control the temperature of the EA-LD. The operating temperature of the EA-LD is set to 45°C to minimize temperature differences from the ambient in the high temperature range; thus the heat absorption is reduced to suppress the power consumption of the TEC. The 1.25 Gbps transmitter uses a distributed feedback laser diode (DFB-LD) with a wavelength of 1.49  $\mu\text{m}$  in the CAN package, and achieves a high optical output in a wide ambient temperature range without any LD temperature control. The receiver uses an avalanche photo diode (APD) in the CAN package with a built-in dual-rate burst-mode pre-amplifier IC<sup>(2)</sup>, which responds to the rate selection signal to switch the current-voltage conversion gain and the response time constant for the automatic gain control (AGC) and automatic threshold control (ATC) to achieve a high sensitivity at both 1.25 Gbps and 10.3 Gbps rates. The APD has distributed bragg reflector (DBR) layers to reflect the light that has not been absorbed by and transmitted through the absorption layer, back to the absorption layer once again. By optimizing these DBR layers, a high sensitivity has been achieved in a wide range of receiving wavelength of 1.26  $\mu\text{m}$  to 1.36  $\mu\text{m}$ <sup>(3)</sup>. The combination and separation of two transmitting and one receiving signal light has been accomplished by a thin-film wavelength division multiplexing (WDM) filter. For the external electrical interface, a flexible printed circuit (FPC) has been used consider-

ing high-speed operation at 10 Gbps and ease of implementation. The optical module is fabricated in a compact size of 24.0 (L) × 20.0 (W) × 9.7 (H) (mm).

### 2.2 Optical design

A major challenge in the development of the triplexer module having two transmitters is to align the two output light beams from the LDs (EA-LD to DFB-LD) simultaneously to the optical fiber (hereinafter referred to as “optical coupling”). In order to optically couple two LDs and the fiber with a high efficiency while ensuring the distance for a WDM filter and an isolator between the optical fiber and each of the two transmission light sources, an optical system with either two or three lenses are required. Our investigation result is summarized in Table 1, which illustrates the two-lens (Fig. 2) and three-lens (Fig. 1) optical systems for comparison. The two-lens system is assumed to be a collimating optical system to ensure the distance between the LD and the fiber as shown in Fig. 2. Figure 3 shows a calculation result for the tolerance of the LD-lens distance versus optical coupling efficiency. In the case of the two-lens optical system, the efficiency is greatly dependent on the LD-lens distance, which must have an accuracy of at least ± 2 μm, whereas in the case of the three-lens optical system, the spot position on the fiber can be adjusted by aligning the LD and lens in the optical axis direction, and thus even with an accuracy of ± 40 μm, the decrease in efficiency is kept

Table 1 Comparison of optical systems

	Two-lens optical system (Collimating optical system)	Three-lens optical system
Allowable tolerance of the LD-lens distance	< ±2 μm ×	< ±40 μm ○
EA-LD optical coupling efficiency	○	○
DFB-LD optical coupling efficiency	×	○

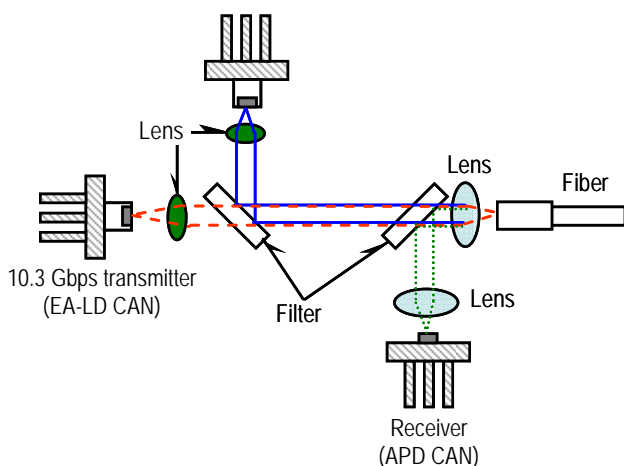


Fig. 2 Two-lens collimating optical system

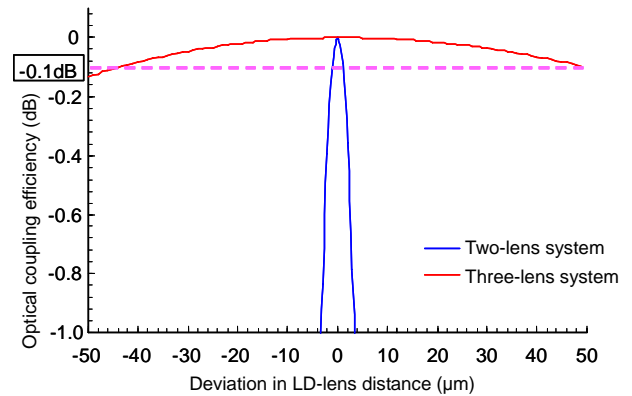


Fig. 3 Optical coupling efficiency versus deviation in the LD-lens distance

to 0.1 dB or less; and a high optical coupling efficiency can be achieved simultaneously for the two LDs. Based on these comparison results, the three-lens optical system was adopted, and optical coupling efficiencies of -2.84 dB and -1.65 dB for the EA-LD and DFB-LD have been achieved, respectively. These results are good enough to satisfy the optical output requirement specified by IEEE 802.3av.

### 3. Evaluation Results

#### 3.1 10.3 Gbps transmitter

Table 2 shows the main characteristics of the 10.3 Gbps transmitter at a case temperature between -5°C and 70°C, which sufficiently satisfy the IEEE 802.3av standard, including a light output of + 4.0 dBm and extinction ratio of 9.1 dB. Figure 4(a) shows an optical output waveform at a case temperature of 25°C (EA-LD temperature of 45°C), and Fig. 4(b) shows an optical waveform after being transmitted over a distance of 25 km in a single mode fiber (SMF). A clear eye-opening with a mask margin of 44% was obtained, and the waveform after transmission had also a clear eye-opening. Deterioration in the sensitivity between before and after the SMF transmission (dispersion penalty) was equal to or less than 0.1 dB over the full temperature range. Figure 5 shows the power consumption of the TEC, which is 0.3 W or less even at a case temperature of 70°C.

Table 2 Main characteristics of 10.3 Gbps transmitter

10.3 Gbps transmitter	IEEE 802.3av PR30 standard	Evaluation result
Transmission light output (dBm)	+2 to +5	+4.0
Extinction ratio (dB)	>6	9.1
Mask margin (%)	-	44
Dispersion penalty (dB)	<1.5	0.1

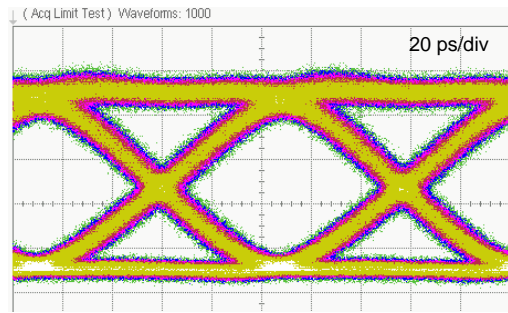
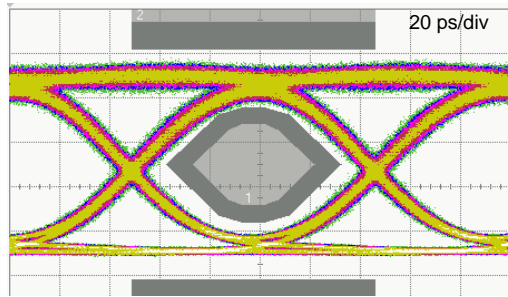


Fig. 4 Optical waveform of 10.3 Gbps transmitter

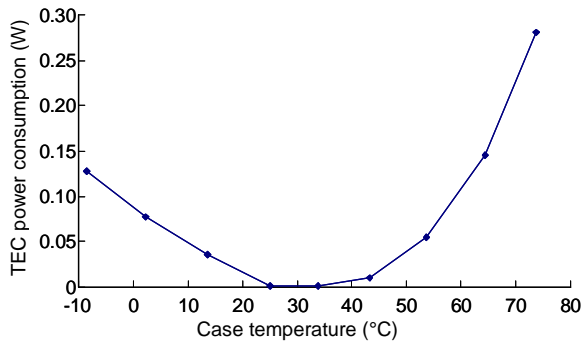


Fig. 5 Power consumption of TEC

### 3.2 1.25 Gbps transmitter

Table 3 shows the main characteristics of the 1.25 Gbps transmitter at a case temperature between  $-5^{\circ}\text{C}$  and  $70^{\circ}\text{C}$ , which sufficiently satisfy the IEEE 802.3ah standard, including a high light output of  $+4.9$  dBm and high extinction ratio of 15.5 dB. Figure 6 shows optical output waveforms at case temperatures of  $-5^{\circ}\text{C}$ ,  $25^{\circ}\text{C}$ , and  $70^{\circ}\text{C}$ . A clear eye-opening was obtained over the full temperature range with a mask margin of 47%. The transmission penalty was equal to or less than 0.03 dB over the full temperature range.

Table 3 Main characteristics of 1.25 Gbps transmitter

1.25 Gbps transmitter	IEEE 802.3ah PX20 standard	Evaluation result
Transmission light output (dBm)	+2 to +7	+4.9
Extinction ratio (dB)	>6	15.5
Mask margin (%)	-	47
Dispersion penalty (dB)	<2.3	0.03

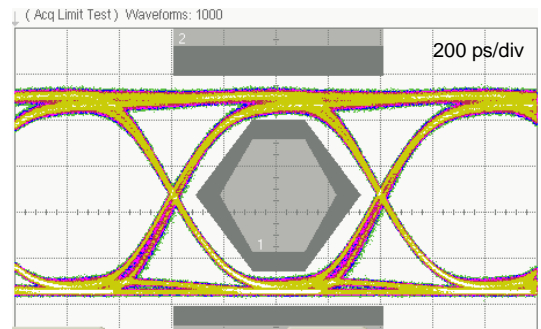
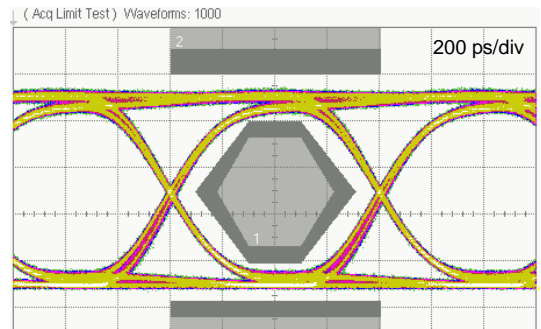
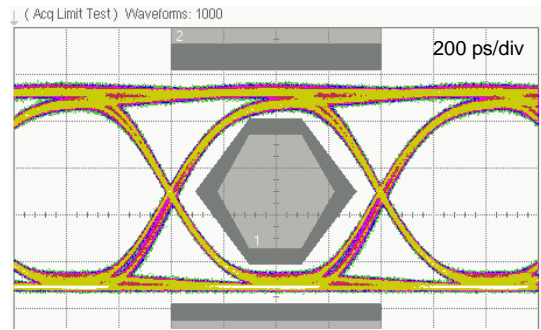


Fig. 6 Optical output waveforms of 1.25 Gbps transmitter

### 3.3 Receiver

Figure 7 shows the wavelength dependence of the APD's DC responsivity at  $25^{\circ}\text{C}$ . As a result of the optimization of DBR, a 0.77 A/W or higher DC responsivity was obtained over a wide range of wavelength from  $1.26\ \mu\text{m}$  to  $1.36\ \mu\text{m}$ . Figure 8 shows the receiver's bit error ratios at case temperatures of  $-5^{\circ}\text{C}$ ,  $25^{\circ}\text{C}$ , and  $70^{\circ}\text{C}$ . The light source used for the evaluation at the bit rate of 10.3 Gbps was  $2^{31}-1$  pseudorandom binary sequence (PRBS) with an extinction ratio of 6 dB and a wavelength of  $1.27\ \mu\text{m}$ . The 10 G-EPON standard assumes the use of forward error correction (FEC) codes, and thus specifies the bit error ratio (BER) to be  $10^{-3}$ . A minimum sensitivity of  $-30.2$  dBm and a maximum sensitivity of  $-6$  dBm were obtained. The light source used for the evaluation of 1.25 Gbps operation was  $2^7-1$  PRBS with an extinction ratio of 9 dB and a wavelength of  $1.27\ \mu\text{m}$ ; and at the BER level of  $10^{-12}$ , a minimum sensitivity of  $-36.0$  dBm and a maximum sensitivity of  $-6$  dBm were obtained. These sensitivity

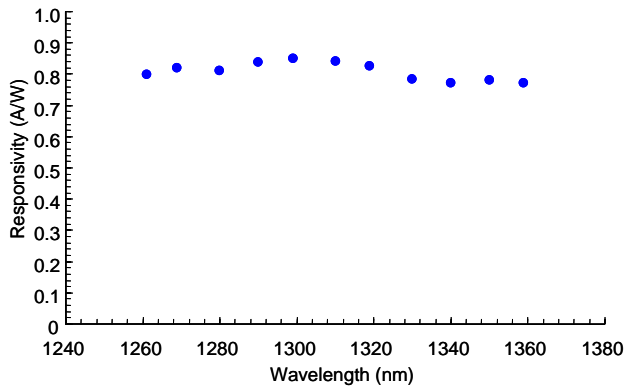


Fig. 7 Wavelength dependence of the APD's DC sensitivity

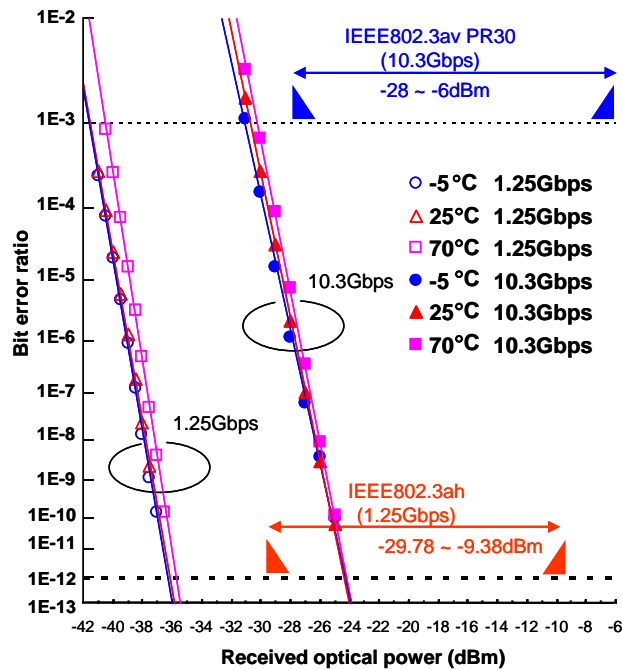


Fig. 8 Bit error rate characteristics of receiver

results of 10.3 Gbps and 1.25 Gbps both satisfy the IEEE 802.3av and IEEE 802.3ah standards.

#### 4. Conclusion

A triplexer module for the 10 G-EPON OLT has been developed with a 10.3 Gbps transmitter, 1.25 Gbps transmitter, and 1.25 Gbps/ 10.3 Gbps receiver integrated. By adopting the three-lens optical system, a high optical coupling efficiency has been achieved for the two LDs, providing sufficiently good output performance to satisfy the IEEE 802.3av standard. In addition, by using a dual rate preamplifier IC and high-sensitivity APD, good sensitivities have been obtained at both the bit rates of 1.25 Gbps and 10.3 Gbps. We expect that the newly developed optical module will help accelerate the spread of the next-generation optical access system.

#### References

- (1) Okada, N., et al.: Cost-Effective 10.7 Gbit/s Cooled TOSA Employing Rectangular TO-CAN Package Operating up to 90°C, OFC/NFOEC Poster Session, JWA38 (2010)
- (2) Masaki Noda, et al.: Dual-rate Burst-mode Preamplifier for 10 G-EPON OLT Receiver, IEICE Society Conference 2010, C-3-41 (2010) (in Japanese)
- (3) Sasahata, Y., et al.: The Development of the 1.27  $\mu\text{m}$  High Responsivity Avalanche Photodiodes for 10G-EPON (OLT), OFC/NFOEC Poster Session, JWA4 (2010)

# High-power 638 nm Semiconductor Laser Diode for Small Color Projectors

Authors: Takehiro Nishida\*, Harumi Nishiguchi\* and Naoyuki Shimada\*

## 1. Introduction

Semiconductor laser diodes (LDs) started to appear in consumer appliances in the 1980s as a light source for compact discs (CD) (wavelength of 780 nm). They expanded in the mid-1990s to the digital versatile disc (DVD) (wavelength of 660 nm), and recently to Blu-ray<sup>1</sup> (wavelength of 405 nm). In addition, applications to optical communication also started in the 1980s using a wavelength between 1.3  $\mu\text{m}$  to 1.6  $\mu\text{m}$ , and LDs are now used for long-distance communication such as intercontinental submarine cables as well as short-distance communication such as local area networks (LAN). All of these usages relate to the same application field, and are associated with the evolution of applications. In other words, these developments are an evolution along the same line already established in the 1980s.

In the meantime, LDs have advantageous features over lamps and light emitting diodes such as high wall plug efficiency (WPE) and small etendue, and thus they are considered to be a suitable light source for display applications, which would make the best use of those features<sup>(1)</sup>. Recently, spatial light modulators (SLMs), LDs for each of the RGB colors, and other elemental technologies required for laser displays have become available<sup>(2) (3) (4) (5)</sup>, which in turn stimulated research and development on laser displays. Currently, much R&D is under way on the application of various displays including small projectors, televisions, head-up displays, and super large cinema projectors, and some manufacturers have already begun releasing such products. Laser displays are likely to create a new application field for LDs, which could be totally different from the previously described applications.

This paper describes the features of the high-power 638 nm range lateral multi-mode LD designed for a red-color light source of these projectors.

## 2. Laser Display and Light Source Laser

### 2.1 Selection of red LD wavelength for laser display

For display applications of motion pictures and still images to be recognized by the human eye, the lasing wavelength of the light source laser is important. In the

red color region, the sensitivity of the human eye decreases as the wavelength increases. Figure 1 shows the photopic luminosity curve in the red color region. A red LD has already been put into practical use for DVD applications. However, this LD requires a high power to obtain a predetermined brightness due to its low luminosity factor, and is not recommended for display use, not only because of its high power consumption but also safety. If the wavelength is made shorter to 638 nm, the luminosity factor is roughly tripled (the same predetermined brightness is obtained by one third of the power compared to 660 nm wavelength).

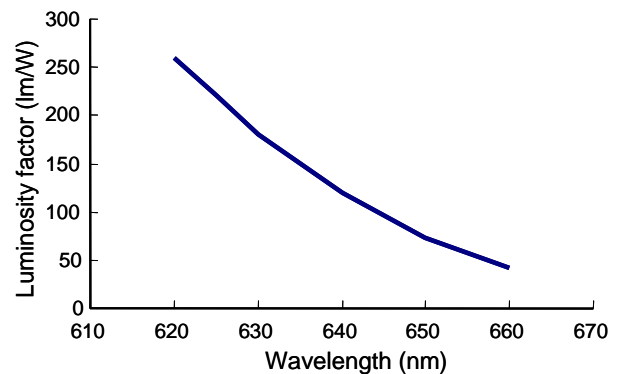


Fig. 1 Relationship between red color wavelength and luminous factor

Most of the LDs that emit light in the red color range are fabricated using AlGaInP materials. However, a heterojunction fabricated by using this type of material has a narrow band offset in the conduction band, which is likely to cause electron overflow from the active layer into the cladding layer, and making high-output operation or high-temperature operation difficult. The maximum band gap in the cladding layer is determined by the material itself; therefore, as the LD's lasing wavelength is made shorter (in other words, the band gap of the active layer is made greater), overflow is more likely to occur and the LD characteristics are more degraded.

In this way, the luminosity factor and LD characteristics have a trade-off relationship. Nevertheless, considering the temperature characteristics, we selected a lasing wavelength of 638 nm.

<sup>1</sup> Blu-ray is the trademark of Blu-ray Disc Association.

## 2.2 Power output improvement of red LD for laser display

For an illumination-type small display with a two-dimensional spatial light modulator such as an imaging device used for a regular projector, a high output LD is desirable and a lateral multi-mode LD is commonly used. A lateral single-mode LD is generally fabricated with a window mirror structure, whereas the broad-area (BA) structure commonly used for lateral multi-mode LDs has a broad active layer, and the light density per unit length in the lateral direction can easily be reduced, and thus non-window-type 500 mW class devices are easily fabricated based on the GaAs active layer structure in the 800 nm to 900 nm infrared light range. However, AlGaInP-based red LDs tend to deteriorate at a relatively low light density. Figure 2 shows P-I characteristics of a BA-type LD without a window, which indicates that an initial catastrophic optical degradation (COD) of approximately 600 mW decreases to 300 mW only after an operation with a relatively low output of 150 mW for 170 hours. Therefore, it is essential even for the BA-type LD to use the window mirror structure to realize a highly reliable red LD<sup>(5)</sup>.

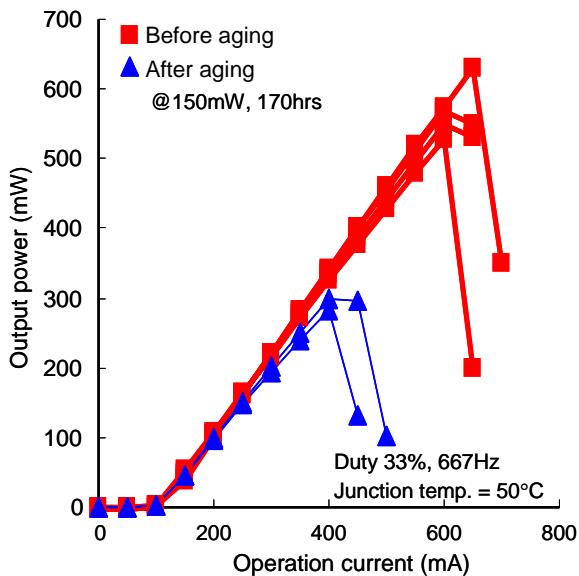


Fig. 2 COD level of multiple mode LDs without window structure

## 3. Device Structure

Figure 3 shows a schematic of the BA-type red LD. The cladding layers are made from AlInP, which has a low refractive index, in order to increase the optical confinement factor  $\Gamma$  of the active layer. The use of AlInP cladding layers is generally considered to give a negative influence on the carrier confinement<sup>(6)</sup>. However, we thought that an increase in the confinement factor  $\Gamma$  obtained by combining the active and the AlInP cladding layers would provide a low threshold current density, resulting in an advantageous effect for the device.

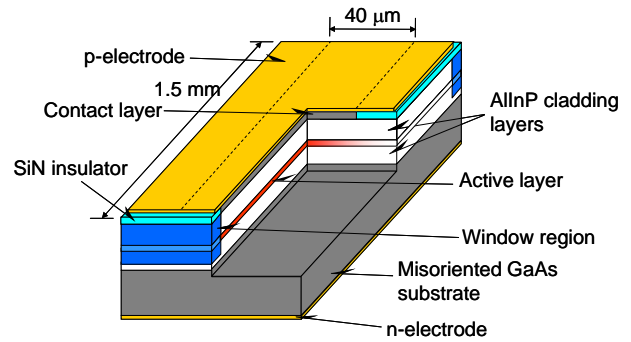


Fig. 3 Structure of BA-type red LD

The stripe structure is of an insulator film stripe, which is commonly used for the BA LD, and the stripe width was set to 40  $\mu\text{m}$ . The window mirror structures are formed by Zn diffusion at the LD facets to prevent them from COD<sup>(7)</sup>. In addition, the front and rear facets are treated with anti-reflection (AR) and high-reflection (HR) coatings, respectively, to cope with the high power operation. The cavity length was designed to be 1.5 mm and assembled into a high heat dissipating open package of 5.6 mm in diameter by the junction down mounting via an aluminum nitride (AlN) submount.

## 4. Laser Characteristics

Figures 4 and 5 respectively show the temperature dependence of the P-I characteristics and the lasing spectrum of the lateral multi-mode LD in pulse operation. The obtained light output power was 1 W or greater up to  $T_c = 50^\circ\text{C}$ , and 800 mW even at  $60^\circ\text{C}$ . The wall plug efficiency was 35% at  $25^\circ\text{C}$  with a light output power of 1 W in continuous wave (CW) operation.

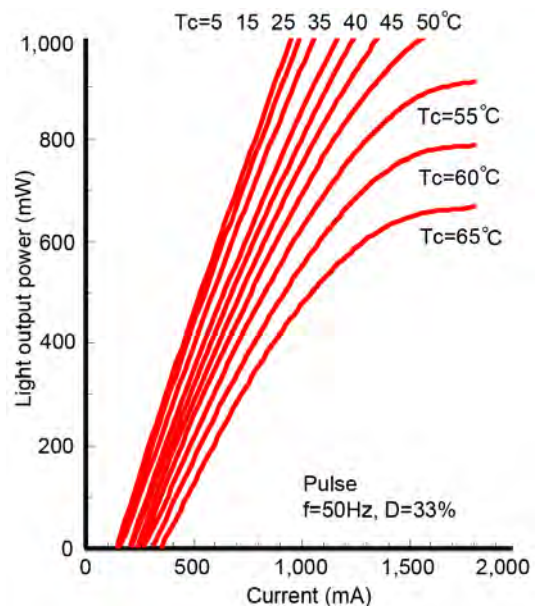


Fig. 4 Temperature dependence of P-I characteristics

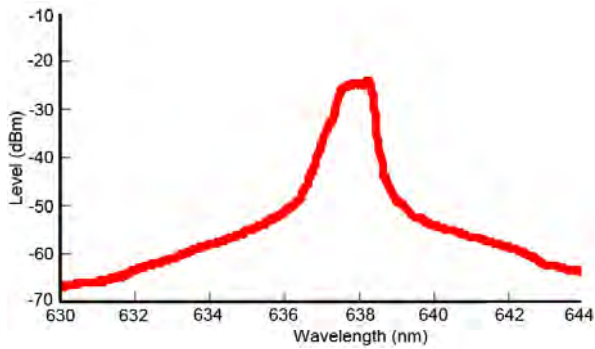


Fig. 5 Lasing spectrum

The lasing wavelength of this LD was 638.3 nm in CW operation at 25°C and 500 mW. For the light sources used in display devices viewed by the human eye, the commonly used physical quantity is luminous flux (unit: lumen) rather than Watt. By using the chart in Fig. 1, an output of 1 W at 638 nm can be converted to a luminous flux of over 120 lumens. The full angle at half maximum of the far field pattern (FFP) is 5 degrees in the horizontal direction and 35 degrees in the vertical direction.

Figure 6 shows the results of life tests in CW operation at  $T_c = 50^\circ\text{C}$  and 1.5 A with automatic current control (ACC). The operation current was adjusted to set the initial light output power to about 1 W. After 1,200 hours, a decrease in the light output power was very small at a level of 10%, and no obvious deterioration was observed including instantaneous degradation due to COD.

The 638 nm red semiconductor LD for laser display applications has achieved an output power of 1 W or more in a wide range of guaranteed operating temperatures up to 50°C, with a high WPE of approximately 35% (at a case temperature of 25°C in 1 W pulse operation), which is, to our best knowledge, the world's highest level light source. The 638 nm light having a high luminous factor enables the configuration of a bright light source of approximately 120 lumen, which is ideal for small projector-type laser displays under severe operating environments.

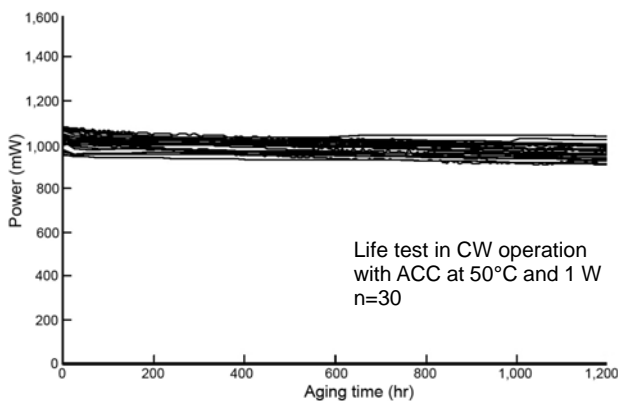


Fig. 6 Life test result

## 5. Conclusion

Small laser projectors, which are connected to or installed in notebook PC or mobile devices, are expected to further evolve and provide a new application for LDs different from the conventional usages. For one of these types of laser displays, i.e., the illumination-type display, a lateral multi-mode LD with a lasing wavelength of 638 nm has been developed. An output power of 1 W or more has been confirmed in a wide range of guaranteed operating temperatures between 5°C and 50°C, which is sufficient for this type of display. In the life test performed with an ACC, the newly developed LD demonstrated stable operation for over 1,200 hours, and is confirmed to be the most suitable for projector-type laser displays.

## References

- (1) Yamamoto, K.: Next-generation LED and laser displays, *Oyo Buturi*, 78, No. 11, 1021 (2009) (in Japanese)
- (2) Yamamoto, K.: Laser Projection Technology, *The Review of Laser Engineering*, 36, 173 (2008) (in Japanese)
- (3) Nakamura, S., et al.: Blue InGaN-based laser diodes with an emission wavelength of 450 nm, *Appl. Phys. Lett.*, 76, No. 1, 22 (2000)
- (4) Enya, Y., et al.: 531 nm Green Lasing of InGaN Based Laser Diodes on Semi-Polar {2021} Free-Standing GaN Substrates, *Appl. Phys. Express* 2, 082101 (2009)
- (5) Nishida, T., et al.: Highly reliable 637–639 nm red high-power LDs for displays, *Proc. SPIE*, 7583, 758303-1 (2010)
- (6) Mowbray, D. J., et al.: Electronic band structure of AlGaInP grown by solid-source molecular-beam epitaxy, *Appl. Phys. Lett.*, 65, No. 2, 213–215 (1994)
- (7) Kaneko, Y., et al.: Refractive indices measurement of (GaInP)<sub>m</sub>/(AlInP)<sub>n</sub> quasi-quaternaries and GaInP/AlInP multiple quantum wells, *J. Appl. Phys.*, 76, No. 3, 1809–1818 (1994)

